Environmental Science & Technology

pubs.acs.org/est

Article

Significant Variability in the Photocatalytic Activity of Natural Titanium-Containing Minerals: Implications for Understanding and Predicting Atmospheric Mineral Dust Photochemistry

Maya Abou-Ghanem, Anton O. Oliynyk, Zhihao Chen, Laura C. Matchett, Devon T. McGrath, Michael J. Katz, Andrew J. Locock, and Sarah A. Styler*

Cite This: *Environ. Sci. Technol.* 2020, 54, 13509−13516

Read Online

ACCESS | Metrics & More | Article Recommendations | Supporting Information

ABSTRACT: The billions of tons of mineral dust released into the atmosphere each year provide an important surface for reaction with gas-phase pollutants. These reactions, which are often enhanced in the presence of light, can change both the gas-phase composition of the atmosphere and the composition and properties of the dust itself. Because dust contains titanium-rich grains, studies of dust photochemistry have largely employed commercial titanium dioxide as a proxy for its photochemically active fraction; to date, however, the validity of this model system has not been empirically determined. Here, for the first time, we directly investigate the photochemistry of the complement of natural titanium-containing minerals most relevant to mineral dust, including anatase, rutile, ilmenite, titanite, and several titanium-bearing species. Using ozone as a model gas-phase pollutant, we show that titanium-containing minerals other than titanium dioxide can also photocatalyze trace gas uptake, that samples of the same mineral phase can display very different reactivity, and that prediction of dust photoreactivity based on elemental/mineralogical analysis and/or light-absorbing properties is challenging. Together, these results show that the photochemistry of atmospheric dust is both richer and more complex than previously considered, and imply that a full understanding of the scope and impact of dust-mediated processes will require the community to engage with this complexity *via* the study of ambient mineral dust samples from diverse source regions.

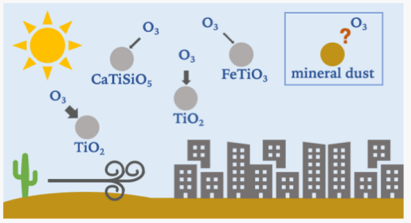

INTRODUCTION

Although each cubic meter of air contains only microgram quantities of particulate matter,[1] these particles have an outsize influence on climate[2] and human health.[3] Mineral dust is one of the most abundant types of atmospheric particulate matter, with over a billion tons emitted into the atmosphere each year from remote arid regions in North Africa, East Asia, and Australia.[4] Once aloft, dust can be transported to urban areas, where it can interact with locally emitted pollutants[5] and thereby influence the composition of the urban atmosphere: for example, observed reductions in mixing ratios of ozone, an important component of urban smog,[6] during periods of elevated dust loadings have been attributed to the scavenging of ozone and its precursor gases (*e.g.*, HNO_3).[7] These interactions can also influence the properties of the dust itself: for example, the reaction of dust with pollutants can change its toxicity,[8] optical properties,[9] cloud condensation nuclei (CCN)[10] and ice nuclei (IN)[11] activity, and its ability to act as a depositional source of soluble iron to marine ecosystems.[12]

Motivated by these diverse impacts, many laboratory studies have examined the kinetics and products of the reaction of mineral dust and mineral dust proxies with both inorganic[13] and organic[14,15] pollutant gases; in many cases, researchers have found these reactions to be enhanced by light.[16] Because mineral dust contains Ti, which is a well-known semiconductor photocatalyst in its oxide form,[17] the atmospheric chemistry community has extensively studied the TiO_2-catalyzed photochemistry of many urban pollutants.[18]

Although the use of TiO_2 enables detailed mechanistic analysis that is challenging for natural dust, the composition of which is complex and variable, it is not without its weaknesses: for example, although the Ti content of mineral dust determined using elemental analysis is typically reported as TiO_2, Ti is also a component of many other minerals detected in atmospheric dust.[19,20] In addition, even in cases where mineralogical analysis has specifically identified TiO_2 in dust samples,[21] there is no guarantee that the reactivity of this TiO_2 is identical across all natural samples or comparable to that of commercially sourced samples, since the surface and band structures of TiO_2 are influenced by many sample-specific properties, including crystal structure,[22] degree of hydration,[23] presence of dopants,[24] and particle size.[25]

Received: August 31, 2020
Revised: September 23, 2020
Accepted: September 24, 2020
Published: October 15, 2020

To improve our understanding of natural mineral photochemistry, we investigated the uptake of ozone by 10 natural Ti-containing minerals, which we chose based on both their Ti content and their environmental abundance. We find that all of these minerals display photoenhanced uptake of ozone, that ozone uptake varies both between and within mineral phases, that ozone uptake does not increase linearly with elemental Ti content, and that commercial TiO_2 is significantly more reactive toward ozone than all of the natural samples studied here. Further, we discuss these observations in the context of comprehensive characterization data, including particle size, morphology, crystallographic structure, band structure, and elemental impurity identification. This approach, which brings together both atmospheric and materials chemistry perspectives, will ultimately enable us to better predict the influence of dust−pollutant interactions on atmospheric composition.

MATERIALS AND METHODS

Experiments were conducted using a set of 10 natural Ti-containing minerals, which we sourced from www.minfind.com and purchased through contact with individual vendors. Details regarding sample purification, preparation, grinding, and characterization *via* X-ray diffraction (XRD; phase identification), electron microprobe analysis (EMPA; Ti content of the dominant mineral phase present in each sample), nitrogen adsorption analysis (specific surface area determination), ultraviolet−visible (UV−vis) diffuse reflectance spectroscopy (optical properties and, where possible, band gap determination), and scanning electron microscopy (SEM; particle size and morphology) are presented in the Supporting Information.

Mineral-coated Pyrex insert tubes were exposed to ozone in a coated-wall atmospheric pressure flow tube reactor, which was mounted in the center of a black plastic box and surrounded by four UV-A lamps (4.13−3.02 eV, eV_{max}: 3.48; 300−410 nm, λ_{max}: 356 nm). With four lamps turned on, the NO_2 photolysis frequency (J_{NO_2})[26] inside the reactor was 0.0045 ± 0.0001 s^{-1}, which is in the range of noontime photolysis frequencies measured at a northern midlatitude site.[27] We note, however, that this comparison does not take into account the spectral mismatch between our lamp emission profiles and the solar radiation spectrum at this location. Further details regarding the flow tube reactor, NO_2 actinometry, insert tube preparation, and experimental protocols are presented in the Supporting Information.

Ozone was introduced to the flow tube by a movable injector; the ozone−surface interaction time was calculated using the volumetric gas flow and the flow tube dimensions, and the pseudo-first-order rate constant for the reaction, k_{obs}, was determined using the following equation[28]

$$[O_3] = [O_3]_0 \times e^{-k_{obs}t} \quad (1)$$

Here, $[O_3]$ is the average steady-state ozone concentration at the exit of the flow tube upon exposure to the mineral substrate under either light or dark conditions, $[O_3]_0$ is the average ozone concentration with the movable injector entirely pushed in (*i.e.*, with no exposure to the mineral substrate), and t is the residence time of ozone inside the mineral-coated section of the flow tube. The obtained k_{obs} values were then used to calculate effective uptake coefficients, γ_{eff}, as follows[28]

$$\gamma_{eff} = \frac{D_{tube} \times k_{obs}}{\omega_{O_3}} \quad (2)$$

Here, D_{tube} is the flow tube diameter and ω_{O_3} is the mean thermal velocity of ozone under our experimental conditions. Finally, γ_{eff} was corrected for gas-phase diffusion limitations[29] and sample-specific surface area scaling (Brunauer−Emmett−Teller; BET) was applied to yield γ_{BET}, which is the value reported in this work[30]

$$\gamma_{corr} = \frac{\gamma_{eff}}{1 - \gamma_{eff}\frac{3}{2N_{Shw}^{eff}Kn}} \quad (3)$$

$$\gamma_{BET} = \gamma_{corr} \times \frac{S_{geo}}{S_{BET} \times m} \quad (4)$$

Here, N_{Shw}^{eff} is the effective Sherwood number, Kn is the Knudsen number, S_{geo} is the geometric surface area of the mineral-coated section of the coated-wall flow tube (m^2), m is the sample mass (g), and S_{BET} is the specific BET surface area ($m^2\ g^{-1}$) of the sample; these values, which are specific for our experimental conditions and the geometry of the coated-wall flow tube, are presented in the Supporting Information.

For both the commercial and natural TiO_2 samples, almost complete depletion of ozone was observed upon illumination; therefore, to minimize diffusion limitations for these samples, we performed experiments using TiO_2/SiO_2 mixtures. This approach required additional considerations for the γ_{BET} calculations, which we present in the Supporting Information. To verify that uptake of ozone was insignificant in the absence of minerals, we conducted blank experiments using empty Pyrex insert tubes (n = 3). In all cases except for one trial of titanite 2 under dark conditions, the loss of ozone in these blank tubes was significantly lower than the loss observed for mineral-coated tubes. For this reason, the γ_{BET} values presented here are not blank-corrected and γ_{BET} values for titanite 2 under dark conditions are not reported.

RESULTS AND DISCUSSION

Selection and Characterization of Ti-Containing Minerals Relevant to Mineral Dust. Our sample set consists of anatase and rutile, two of the three naturally occurring TiO_2 polymorphs (the third, brookite, is uncommon);[31] ilmenite, an iron−titanium oxide commonly found in igneous and metamorphic rocks;[32] titanite, the most abundant titanosilicate;[33] and the titanium-bearing minerals phlogopite, hastingsite, augite, and epidote, which are commonly found members of the mica, amphibole, pyroxene, and epidote supergroups, respectively.[20,34] To assess the extent to which photochemistry varies within a single mineral class, we studied two samples of both anatase and titanite. The mineral names, simplified chemical formulas, geographic origins, and elemental Ti contents of our sample set are displayed in Table 1.

Photoenhanced Ozone Uptake by Ti-Containing Minerals Varies by Several Orders of Magnitude. We investigated the uptake of ozone by Ti-containing minerals using a custom-built coated-wall photochemical flow tube reactor (Figure S1), in which ozone passes through a Pyrex tube coated with the mineral sample of interest and the loss of ozone measured at the outlet of the tube reflects the degree of surface reaction. All mineral samples were exposed to ozone under both dark and illuminated conditions; a representative ozone reaction profile is shown in Figure 1 for titanite 1, and reaction profiles for all other minerals are shown in Figures S3 and S4. In all cases, ozone loss was higher upon illumination

https://dx.doi.org/10.1021/acs.est.0c05861
Environ. Sci. Technol. 2020, 54, 13509−13516

Table 1. Ti and Ti-Bearing Minerals Under Study

mineral	simplified chemical formula	origin	Ti content (mass %)[a]
anatase (commercial)	TiO_2	Sigma-Aldrich	99.8[b]
anatase 1	TiO_2	Pakistan	99.5 ± 0.3
anatase 2	TiO_2	Brazil	99.8 ± 0.2
rutile	TiO_2	Brazil	98.8 ± 0.1
ilmenite	$FeTiO_3$	United States	51.0 ± 1.2
titanite 1	$CaTiSiO_5$	Canada	34.7 ± 0.2
titanite 2	$CaTiSiO_5$	Brazil	38.5 ± 0.2
phlogopite	$KMg_3(AlSi_3O_{10})(F,OH)_2$	Canada	1.02 ± 0.05
hastingsite	$NaCa_2(Mg_4Fe^{3+})(Si_6Al_2)O_{22}(OH)_2$	United States	0.79 ± 0.03
augite	$(Ca,Na)(Mg,Fe,Al,Ti)(Si,Al)_2O_6$	United States	0.71 ± 0.08
epidote	$Ca_2(Al,Fe)_2Si_3O_{12}(OH)$	Norway	0.21 ± 0.02

[a]Reported as TiO_2 by mass; in all cases except commercial anatase, the dominant mineral phase was selected for spot analysis. [b]Reported as TiO_2 by the supplier (Sigma-Aldrich).

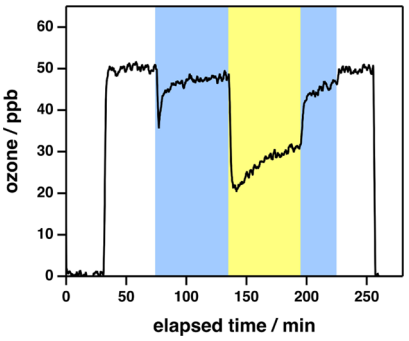

Figure 1. Reaction profile of ozone with titanite 1 at 25% RH. The unshaded regions of the profile denote time periods in which ozone was not exposed to titanite 1. The blue and yellow regions of the profile denote the exposure of ozone to titanite 1 under dark and illuminated conditions, respectively.

and higher than in the absence of mineral samples, which implies the existence of a light-mediated pathway for ozone loss at the surface of all samples. To our knowledge, these results are the first demonstration of photoenhanced trace gas uptake by natural Ti-containing minerals.

For each mineral sample, the γ_{BET} values under illumination are higher than those under dark conditions; these values are presented in Figures 2 (illuminated conditions) and S14 (dark conditions). As illustrated in Figure 2, γ_{BET} values for illuminated samples span four orders of magnitude, ranging from $(1.8 \pm 0.3) \times 10^{-4}$ for commercial TiO_2 to $(1.2 \pm 0.5) \times 10^{-7}$ for epidote. It is not surprising that the TiO_2 minerals (anatase 1, anatase 2, and rutile) are the natural samples with the highest γ_{BET} values, given that TiO_2 is a well-known semiconductor photocatalyst with band gaps in the near-UV for both its anatase and rutile phases.[35] In their study of ozone decomposition at the surface of mixed TiO_2−SiO_2 films, Nicolas et al. drew from studies of the behavior of ozone in aqueous systems (see *e.g.*, Staehelin and Hoigné[36]) to propose a mechanism for the TiO_2-catalyzed uptake of ozone.[37] In this mechanism, which is described in detail in the Supporting Information, absorption of light with energy equal to or greater than the band gap of TiO_2 leads to the release of molecular oxygen.

Since the light-enhanced uptake of ozone has not been previously explored for Ti-containing minerals other than TiO_2, no specific mechanisms currently exist to explain the reactivity of the remaining minerals in our sample set. To assess if these minerals have the potential to be semiconductor photocatalysts, we obtained diffuse reflectance spectra for each sample, which we then transformed using the Kubelka−Munk function as described in the Supporting Information. As shown in Figures 3 and S13, all of the mineral samples investigated in this study absorb light in the emission range of the UV-A lamps used in the photoreactor and many have band gaps that lie within this emission range. Therefore, the non-TiO_2 minerals in our sample set can, in principle, catalyze the photoreduction of ozone *via* the mechanism proposed for TiO_2. However, as shown in Figure 2, these samples are significantly less photoactive than the TiO_2 minerals, which for a given mineral sample may reflect considerations such as the extent of its band gap overlap with the emission range of the UV-A lamps; the absolute position of its conduction/valence

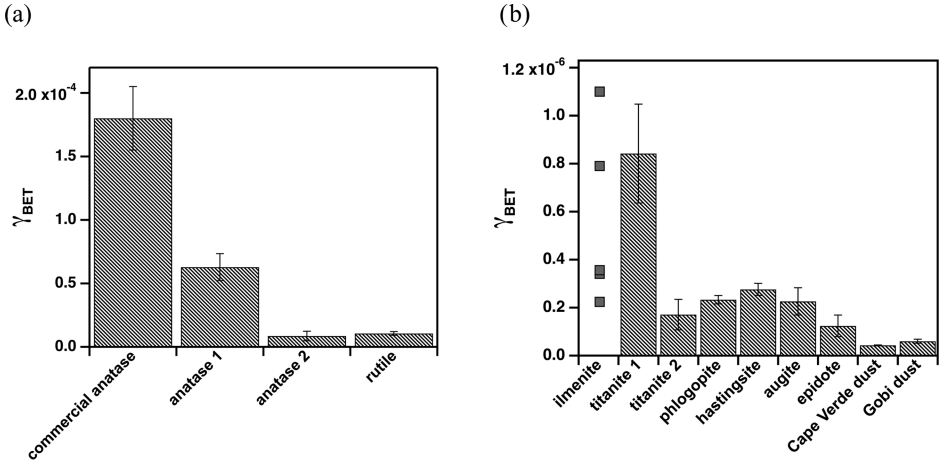

Figure 2. BET uptake coefficients (γ_{BET}) for ozone at RH 25% at the surface of illuminated (a) commercial and natural TiO_2 and (b) other Ti minerals, Ti-bearing minerals, and desert dust samples (Cape Verde depositional dust and Gobi dust). For all samples except ilmenite, each data point represents the mean of three trials, with 1σ error bars; for ilmenite, which appeared to display bimodal reactivity (see the Supporting Information), each trial (n = 6) is displayed individually.

https://dx.doi.org/10.1021/acs.est.0c05861
Environ. Sci. Technol. 2020, 54, 13509−13516

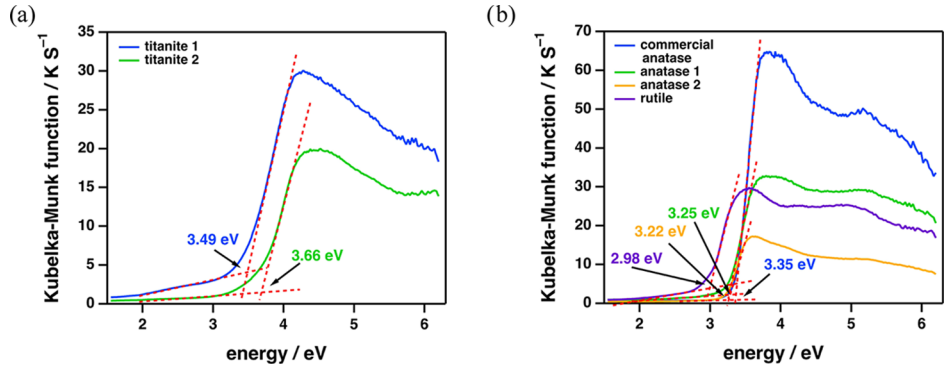

Figure 3. Diffuse reflectance UV−vis spectra (displayed in Kubelka−Munk units) for (a) titanite samples and (b) TiO_2 minerals. The intersection of the dashed red lines for each sample indicates the position of the band gap.

band edges in comparison to the redox potential of the relevant adsorbed species (*i.e.*, oxygen and/or ozone);[38] and its interfacial charge transfer efficiency, which in turn reflects the competition between electron−hole recombination and charge transfer to adsorbed species.[17]

As described in the Supporting Information, the catalytic uptake of ozone by metal oxides under dark conditions is thought to be mediated by reactive Lewis acid surface sites (SS).[39] In particular, the interaction of ozone with these sites has been proposed to lead to the formation of gas-phase molecular oxygen and adsorbed atomic oxygen (SS−O), the latter of which can subsequently react with ozone or another adsorbed oxygen atom to regenerate the surface sites.[40,41] In this context, we propose that the photocatalytic loss of ozone in our experiments may also occur *via* photocleavage of the SS−O bond, which would also regenerate reactive surface sites and thus enable sustained ozone uptake. Since the photocleavage potential of this bond would depend on the strength of the SS−O interaction, and thus be sample-specific,[39] this mechanism would also explain the sample-to-sample variability in ozone uptake coefficients apparent in Figure 2. Although we expect the semiconductor photocatalysis mechanism described in the Supporting Information to dominate for the TiO_2 minerals, we note that if these minerals also possess strong SS−O bonds, which would limit surface site regeneration, then SS−O photocleavage would also lead to enhanced ozone uptake upon illumination for these samples. We suggest that further studies of the mechanism of ozone photochemistry at mineral surfaces would benefit from surface spectroscopic measurements of ozone binding frequencies,[39,42] which have previously been shown to provide insight into the influence of molecular geometry and symmetry on the photochemistry of adsorbed species.[43]

Samples of the Same Mineral Phase Exhibit Significantly Different Photoreactivities. Interestingly, as shown in Figure 2, we find significantly different photoreactivities for two titanite samples originating from different locations. These observations may reflect differences in the optical properties of the two samples: as shown in Figure 3, the band gap of titanite 1 (3.49 eV; 355 nm) is smaller than that of titanite 2 (3.66 eV; 339 nm), and in particular overlaps the maximum emission wavelength of the UV lamps used in this study (3.48 eV; 356 nm), which enables it to absorb a greater fraction of emitted light in the flow tube reactor.

As shown in Tables S9 and S10, the primary compositional difference between the two titanite samples is that the Fe content of titanite 1 is considerably higher than that of titanite 2. Although no studies have investigated the influence of Fe content on titanite photocatalysis, Fe doping of TiO_2 nanoparticles has been shown to result in band gap energy reductions.[44] In this context, we tentatively attribute the red shift in the band gap of titanite 1 to substitution of Ti by Fe in its crystal structure. Fe doping has also been found to reduce the charge-carrier recombination rate for TiO_2 nanoparticles and thereby increase the probability that photogenerated electrons and holes will react with adsorbed species.[45] If Fe doping affects titanite similarly, then this mechanism would also explain the elevated reactivity observed for titanite 1 with respect to titanite 2.

We also observe significant differences in photoreactivity for the two anatase samples employed in this study: as shown in Figure 2, γ_{BET} for illuminated anatase 1 is more than 7× larger than that of anatase 2. In this case, the explanations employed for the titanite samples do not suffice: despite their different photoreactivities, the two anatase samples have similar band gaps (Figure 3), elemental compositions (Tables S5 and S6), and X-ray diffractogram peak positions (Figure S9). Because we identified only the dominant phase for each mineral using EMPA and XRD, we cannot assess the extent to which dopants[24] (*e.g.*, trace Nb and Fe, the quantities of which vary for these two samples) and/or intergrown mineral phases[46] present at trace levels may have influenced the photoreactivity of these samples. In the following paragraphs, we consider several additional factors that may have contributed to the observed differences in reactivity.

The photocatalytic potential of TiO_2 is influenced by particle size, which controls the available surface area for reactions to occur. In this context, as noted above, we scaled all uptake coefficients to the BET surface area of each mineral. Particle size can also influence the surface acidity[47] and inherent photoreactivity of semiconductors (*e.g.*, by changing the charge-carrier recombination rate[25] and mechanism of electron transport[48]); for these reasons, we used field emission scanning electron microscopy (FESEM) to image a subset of the samples (all TiO_2 samples and both titanite samples). As illustrated in Figure S12, although we found commercial TiO_2 particles to be much smaller and more spherical than the natural mineral samples, we did not see any obvious size distribution differences for the natural samples, which implies that the photoreactivity differences observed for our anatase samples did not arise from sample preparation (*i.e.*, hand grinding) artifacts.

The photoreactivity of TiO_2 can be influenced by many additional factors, including crystal facet[49]; electron mobility[50];

https://dx.doi.org/10.1021/acs.est.0c05861
Environ. Sci. Technol. 2020, 54, 13509−13516

interfacial charge-carrier dynamics[24]; amorphous/crystalline content[51]; exposure of fresh, active surfaces upon grinding[52]; and the amount of surface-sorbed water, which can alter the symmetry of adsorbed species and thereby modify the relative importance of subsequent surface photochemical pathways.[43] As a result of this complexity, predicting and understanding differences in photocatalytic activity is challenging even for synthesized TiO_2 samples.[53] In the natural environment, where a given mineral phase can exhibit a range of elemental substitutions and crystal lattice parameters,[32] the situation is even more complex; nevertheless, we suggest that some/all of these factors may have also been in operation for our samples.

Implications for the Study of Atmospheric Mineral Dust Photochemistry. Studies of mineral dust photochemistry performed to date have largely assumed that Ti present in mineral dust exists solely as TiO_2, and therefore that the photoactive potential of a given dust sample can be predicted using elemental analysis.[18,37,54] To assess the validity of this approach, we first plotted the ozone photoreactivity (γ_{BET}) of our mineral samples as a function of the Ti content of their dominant mineral phase. As illustrated in Figure 4,

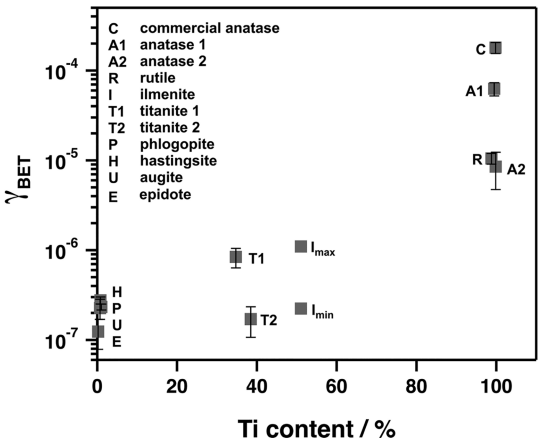

Figure 4. BET uptake coefficients (γ_{BET}) for ozone at the surface of all Ti-containing minerals as a function of the Ti content of each mineral, with the latter obtained as described in Table 1. For all samples except ilmenite, each data point represents the mean of three trials, with 1σ error bars; for ilmenite, which appeared to display bimodal reactivity (see the Supporting Information), the minimum and maximum γ_{BET} values are shown.

although γ_{BET} generally increases with Ti content, this increase is not linear; in addition, we observe substantial variability in γ_{BET} values for all mineral types (*i.e.*, TiO_2 minerals, non-TiO_2 Ti minerals with intermediate Ti content, and Ti-bearing minerals with low Ti content). To explicitly test the validity of elemental analysis-based predictions of dust photoreactivity, we also investigated the uptake of ozone at the surface of two natural mineral dust samples: Cape Verde depositional dust (4.5% Ti)[55] and Gobi dust (1.3% Ti).[14] If the Ti in these samples were present exclusively as TiO_2, with an assumed γ_{BET} range of 6.2×10^{-6}–7.4×10^{-5} (the γ_{BET} values for all replicates of the three natural TiO_2 samples shown in Figure 2), then we would expect γ_{eff} values in the range of 1.8×10^{-6}–5.3×10^{-5} and 5.6×10^{-7}–1.7×10^{-5} for Cape Verde and Gobi dusts, respectively. Although the γ_{eff} values for Cape Verde and Gobi dusts obtained in this work ($(6.4 \pm 0.7) \times 10^{-6}$ and $(2.7 \pm 0.4) \times 10^{-6}$, respectively) fall within the lower bound of these broad ranges, this approach also assumes that the Ti in these samples is present in grains with specific surface areas identical to those of the hand-ground TiO_2 samples studied here, which may not be the case. In addition, these γ_{eff} values are much smaller than those predicted from the results obtained for commercial anatase ($(2.9–3.8) \times 10^{-4}$ and $(0.9–1.2) \times 10^{-4}$ for Cape Verde and Gobi dusts, respectively). Together, these results highlight the limitations of both elemental and mineralogical analyses in predicting mineral dust photoreactivity and provide the first direct evidence that the use of commercial TiO_2 as a proxy for the photoactive component of mineral dust can lead to overestimates in the magnitude of light-mediated processes at the surface of ambient dust.

Climate change is predicted to exacerbate mineral dust emissions;[56] in this context, it is increasingly important to understand the influence of dust on climate, air quality, and health. The atmospheric chemistry community has employed elemental and/or mineralogical analysis to quantify dust nutrient inputs to oceanic ecosystems,[57] determine source regions of ambient dust aerosol,[58] and identify mineral phases important for ice nucleation[59] and trace gas chemistry at the soil surface.[60] Our results highlight for the first time that dust photochemistry does not easily lend itself to these types of bottom-up approaches: specifically, we show that Ti-containing minerals other than TiO_2 photocatalyze trace gas uptake, that dust photochemistry does not scale linearly with elemental Ti content, and that samples of the same mineral phase can exhibit significantly different photoreactivity. To address these limitations, we propose instead a top-down approach, in which the photoactive potential of dust is assessed using samples collected from global source regions representing a diverse range of mineralogical compositions.[61] Because this expanded approach does not make assumptions regarding the components of dust that drive its reactivity, it has the added benefit of considering contributions from both known (*e.g.*, iron oxides[62,63]) and as-yet unidentified photoactive species present in mineral dust.

■ ASSOCIATED CONTENT

Supporting Information

The Supporting Information is available free of charge at https://pubs.acs.org/doi/10.1021/acs.est.0c05861.

Details and characterization of the photochemical coated-wall flow tube reactor; experimental protocol and uptake coefficient calculations; details regarding sample treatment, preparation, and characterization *via* nitrogen adsorption analysis, electron microprobe analysis, X-ray diffraction analysis, UV–vis diffuse reflectance spectroscopy, and scanning electron microscopy; results and discussion for ozone uptake by Ti-containing minerals under dark conditions; mechanistic discussions, comparison to previous literature, and influence of relative humidity for ozone uptake by Ti-containing minerals under light conditions; and additional figures and tables, including schematic and parameters of the photochemical coated-wall flow tube reactor, actinometry data, representative reaction profiles of ozone with Ti-containing minerals, photographs of natural minerals, X-ray diffractograms, UV–vis diffuse reflectance spectra, and scanning electron microscopy images (PDF)

https://dx.doi.org/10.1021/acs.est.0c05861
Environ. Sci. Technol. 2020, 54, 13509–13516

AUTHOR INFORMATION

Corresponding Author

Sarah A. Styler − *Department of Chemistry, University of Alberta, Edmonton, Alberta T6G 2G2, Canada; Now at Department of Chemistry and Chemical Biology, McMaster University, Hamilton, Ontario L8S 4M1, Canada;* orcid.org/0000-0002-6078-9387; Email: stylers@mcmaster.ca

Authors

Maya Abou-Ghanem − *Department of Chemistry, University of Alberta, Edmonton, Alberta T6G 2G2, Canada;* orcid.org/0000-0003-1417-8937

Anton O. Oliynyk − *Department of Chemistry, University of Alberta, Edmonton, Alberta T6G 2G2, Canada; Now at Chemistry and Biochemistry Department, Manhattan College, New York, New York 10471, United States;* orcid.org/0000-0003-0732-7340

Zhihao Chen − *Department of Chemistry, University of Alberta, Edmonton, Alberta T6G 2G2, Canada*

Laura C. Matchett − *Department of Chemistry, University of Alberta, Edmonton, Alberta T6G 2G2, Canada; Now at Department of Chemistry and Chemical Biology, McMaster University, Hamilton, Ontario L8S 4L8, Canada*

Devon T. McGrath − *Department of Chemistry, Memorial University of Newfoundland, St. John's, Newfoundland and Labrador A1B 3X7, Canada*

Michael J. Katz − *Department of Chemistry, Memorial University of Newfoundland, St. John's, Newfoundland and Labrador A1B 3X7, Canada*

Andrew J. Locock − *Department of Earth and Atmospheric Sciences, University of Alberta, Edmonton, Alberta T6G 2G2, Canada*

Complete contact information is available at: https://pubs.acs.org/10.1021/acs.est.0c05861

Author Contributions

M.A.-G. designed and conducted the flow tube experiments with assistance from Z.C. and L.C.M., and guidance from S.A.S. A.O.O. assisted with interpretation of XRD data. A.J.L. quantified elemental composition of mineral samples using EMPA. D.T.M. and M.J.K. performed BET analysis. M.A.-G. and S.A.S. interpreted experimental data and wrote the manuscript, with critical comments from A.O.O., A.J.L., and M.J.K.

Funding

The authors acknowledge the Department of Chemistry and the Faculty of Science at the University of Alberta for start-up funding, the Natural Sciences and Engineering Research Council of Canada (NSERC) for funding through the Discovery Grant program, the Canada Foundation for Innovation (CFI) for funding through the John R. Evans Leaders Fund, and the Alberta Ministry of Economic Development and Trade for funding through the Small Equipment Grants stream of the Research Capacity Program.

Notes

The authors declare no competing financial interest.

No unexpected or unusually high safety hazards were encountered in this work.

ACKNOWLEDGMENTS

This research was undertaken, in part, thanks to funding from the Canada Research Chairs program. The authors thank Vincent Bizon, Paul Crothers, Dirk Kelm, Andrew Hillier, and Jason Dibbs for the construction of the photochemical coated-wall flow tube apparatus employed in these experiments; Drs. Manolis Romanias and Jason Olfert for flow tube design recommendations; Andrew Hillier, Kaiser Leung, Rick Conrad, and Drs. Elijah Schnitzler and Jason Olfert for assistance with construction and programming of relative humidity and temperature sensors; Sherry Gao for assistance with LabView programming for data acquisition; Katie Nichols for assistance with mineral phase identification; and Yi Cai and Brett Wickware for sample preparation and experimental assistance. The authors thank Drs. John N. Crowley and Manolis N. Romanias for donation of the Cape Verde and Gobi dust samples, respectively.

REFERENCES

(1) Hand, J. L.; Gill, T. E.; Schichtel, B. A. Urban and Rural Coarse Aerosol Mass across the United States: Spatial and Seasonal Variability and Long-Term Trends. *Atmos. Environ.* **2019**, *218*, No. 117025.

(2) Myhre, G.; Shindell, D.; Bréon, F.-M.; Collins, W.; Fuglestvedt, J.; Huang, J.; Koch, D.; Lamarque, J.-F.; Lee, D.; Medoza, B.; Nakajima, T.; Robock, A.; Stephens, G.; Takemura, T.; Zhang, H.. Anthropogenic and Natural Radiative Forcing. In *Climate Change 2013: The Physical Science Basis. Contribution of Working Group I to the Fifth Assessment Report of the Intergovernmental Panel on Climate Change*; Stocker, T. F., Qin, D., Plattner, G.-K., Tignor, M., Allen, S. K., Boschung, J., Nauels, A., Xia, Y., Bex, V., Midgley, P. M., Eds.; Cambridge University Press, 2014, pp 659−740.

(3) World Health Organization. *Ambient Air Pollution: A Global Assessment of Exposure and Burden of Disease*; World Health Organization, 2016. https://apps.who.int/iris/handle/10665/250141.

(4) Tanaka, T. Y.; Chiba, M. A Numerical Study of the Contributions of Dust Source Regions to the Global Dust Budget. *Global Planet. Change* **2006**, *52*, 88−104.

(5) Pan, X.; Uno, I.; Wang, Z.; Nishizawa, T.; Sugimoto, N.; Yamamoto, S.; Kobayashi, H.; Sun, Y.; Fu, P.; Tang, X.; Wang, Z. Real-Time Observational Evidence of Changing Asian Dust Morphology with the Mixing of Heavy Anthropogenic Pollution. *Sci. Rep.* **2017**, *7*, No. 335.

(6) Sillman, S. Tropospheric Ozone and Photochemical Smog Environmental Geochemistry. In *Environmental Geochemistry*; Sherwood Lollar, B., Ed.; Elsevier Science, 2003; Vol. *9*, pp 407−431.

(7) de Reus, M.; Dentener, F.; Thomas, A.; Borrmann, S.; Ström, J.; Lelieveld, J. Airborne Observations of Dust Aerosol over the North Atlantic Ocean during ACE 2: Indications for Heterogeneous Ozone Destruction. *J. Geophys. Res.: Atmos.* **2000**, *105*, 15263−15275.

(8) Kameda, T.; Azumi, E.; Fukushima, A.; Tang, N.; Matsuki, A.; Kamiya, Y.; Toriba, A.; Hayakawa, K. Mineral Dust Aerosols Promote the Formation of Toxic Nitropolycyclic Aromatic Compounds. *Sci. Rep.* **2016**, *6*, No. 24427.

(9) Alexander, J. M.; Grassian, V. H.; Young, M. A.; Kleiber, P. D. Optical Properties of Selected Components of Mineral Dust Aerosol Processed with Organic Acids and Humic Material. *J. Geophys. Res.: Atmos.* **2015**, *120*, 2437−2452.

(10) Sullivan, R. C.; Moore, M. J. K.; Petters, M. D.; Kreidenweis, S. M.; Roberts, G. C.; Prather, K. A. Effect of Chemical Mixing State on the Hygroscopicity and Cloud Nucleation Properties of Calcium Mineral Dust Particles. *Atmos. Chem. Phys.* **2009**, *9*, 3303−3316.

(11) Möhler, O.; Benz, S.; Saathoff, H.; Schnaiter, M.; Wagner, R.; Schneider, J.; Walter, S.; Ebert, V.; Wagner, S. The Effect of Organic Coating on the Heterogeneous Ice Nucleation Efficiency of Mineral Dust Aerosols. *Environ. Res. Lett.* **2008**, *3*, No. 025007.

(12) Shi, Z.; Krom, M. D.; Jickells, T. D.; Bonneville, S.; Carslaw, K. S.; Mihalopoulos, N.; Baker, A. R.; Benning, L. G. Impacts on Iron Solubility in the Mineral Dust by Processes in the Source Region and the Atmosphere: A Review. *Aeolian Res.* **2012**, *5*, 21−42.
(13) Tang, M.; Huang, X.; Lu, K.; Ge, M.; Li, Y.; Cheng, P.; Zhu, T.; Ding, A.; Zhang, Y.; Gligorovski, S.; Song, W.; Ding, X.; Bi, X.; Wang, X. Heterogeneous Reactions of Mineral Dust Aerosol: Implications for Tropospheric Oxidation Capacity. *Atmos. Chem. Phys.* **2017**, *17*, 11727−11777.
(14) Romanias, M. N.; Ourrad, H.; Thévenet, F.; Riffault, V. Investigating the Heterogeneous Interaction of VOCs with Natural Atmospheric Particles: Adsorption of Limonene and Toluene on Saharan Mineral Dusts. *J. Phys. Chem. A* **2016**, *120*, 1197−1212.
(15) Carlos-Cuellar, S.; Li, P.; Christensen, A. P.; Krueger, B. J.; Burrichter, C.; Grassian, V. H. Heterogeneous Uptake Kinetics of Volatile Organic Compounds on Oxide Surfaces Using a Knudsen Cell Reactor: Adsorption of Acetic Acid, Formaldehyde, and Methanol on α-Fe_2O_3, α-Al_2O_3, and SiO_2. *J. Phys. Chem. A* **2003**, *107*, 4250−4261.
(16) George, C.; Ammann, M.; D'Anna, B.; Donaldson, D. J.; Nizkorodov, S. A. Heterogeneous Photochemistry in the Atmosphere. *Chem. Rev.* **2015**, *115*, 4218−4258.
(17) Hoffmann, M. R.; Martin, S. T.; Choi, W.; Bahnemann, D. W. Environmental Applications of Semiconductor Photocatalysis. *Chem. Rev.* **1995**, *95*, 69−96.
(18) Chen, H.; Nanayakkara, C. E.; Grassian, V. H. Titanium Dioxide Photocatalysis in Atmospheric Chemistry. *Chem. Rev.* **2012**, *112*, 5919−5948.
(19) Klein, C. Rocks, minerals, and a dusty world. *Health Effects of Mineral Dust* **1993**, *28*, 7−60.
(20) Fitzpatrick, R. W.; Chittleborough, D. J. Titanium and Zirconium Minerals. In *Soil Mineralogy with Environmental Applications*; Dixon, J. B.; Schulze, D. G., Eds.; Soil Science Society of America, Inc.: Madison, Wisconsin, 2002; Vol. 7, pp 667−690.
(21) Engelbrecht, J. P.; McDonald, E. V.; Gillies, J. A.; Jayanty, R. K. M.; Casuccio, G.; Gertler, A. W. Characterizing Mineral Dusts and Other Aerosols from the Middle East—Part 2: Grab Samples and Re-Suspensions. *Inhalation Toxicol.* **2009**, *21*, 327−336.
(22) Zhang, J.; Zhou, P.; Liu, J.; Yu, J. New Understanding of the Difference of Photocatalytic Activity among Anatase, Rutile and Brookite TiO_2. *Phys. Chem. Chem. Phys.* **2014**, *16*, 20382−20386.
(23) Folli, A.; Campbell, S. B.; Anderson, J. A.; Macphee, D. E. Role of TiO_2 Surface Hydration on NO Oxidation Photo-Activity. *J. Photochem. Photobiol., A* **2011**, *220*, 85−93.
(24) Kumar, S. G.; Devi, L. G. Review on Modified TiO_2 Photocatalysis under UV/Visible Light: Selected Results and Related Mechanisms on Interfacial Charge Carrier Transfer Dynamics. *J. Phys. Chem. A* **2011**, *115*, 13211−13241.
(25) Sieland, F.; Schneider, J.; Bahnemann, W. D. Photocatalytic Activity and Charge Carrier Dynamics of TiO_2 Powders with a Binary Particle Size Distribution. *Phys. Chem. Chem. Phys.* **2018**, *20*, 8119−8132.
(26) Zafonte, L.; Rieger, P. L.; Holmes, J. R. Nitrogen Dioxide Photolysis in the Los Angeles Atmosphere. *Environ. Sci. Technol.* **1977**, *11*, 483−487.
(27) Michoud, V.; Colomb, A.; Borbon, A.; Miet, K.; Beekmann, M.; Camredon, M.; Aumont, B.; Perrier, S.; Zapf, P.; Siour, G.; Ait-Helal, W.; Afif, C.; Kukui, A.; Furger, M.; Dupont, J. C.; Haeffelin, M.; Doussin, J. F. Study of the Unknown HONO Daytime Source at a European Suburban Site during the MEGAPOLI Summer and Winter Field Campaigns. *Atmos. Chem. Phys.* **2014**, *14*, 2805−2822.
(28) Pöschl, U.; Rudich, Y.; Ammann, M. Kinetic Model Framework for Aerosol and Cloud Surface Chemistry and Gas-Particle Interactions−Part 1: General Equations, Parameters, and Terminology. *Atmos. Chem. Phys.* **2007**, *7*, 5989−6023.
(29) Knopf, D. A.; Pöschl, U.; Shiraiwa, M. Radial Diffusion and Penetration of Gas Molecules and Aerosol Particles through Laminar Flow Reactors, Denuders, and Sampling Tubes. *Anal. Chem.* **2015**, *87*, 3746−3754.
(30) Michel, A. E.; Usher, C. R.; Grassian, V. H. Reactive Uptake of Ozone on Mineral Oxides and Mineral Dusts. *Atmos. Environ.* **2003**, *37*, 3201−3211.
(31) Jaffe, H. W. *Crystal Chemistry and Refractivity*; Dover Publications, Inc.: Mineola, New York, 1996.
(32) *Rock-Forming Minerals Vol. 5A: Non-Silicates: Oxides, Hydroxides and Sulphides*, 2nd ed.; Bowles, J. F. W., Howie, R. A., Vaughan, D. J., Zussman, J., Eds.; The Geological Society Publishing House: Bath, United Kingdom, 2002.
(33) Clarke, F. W.; Washington, H. S. *The Composition of the Earth's Crust*; U.S. Government Printing Office, 1924.
(34) Franz, G.; Liebscher, A. Physical and Chemical Properties of the Epidote Minerals−an Introduction. *Rev. Mineral. Geochem.* **2004**, *56*, 1−81.
(35) Reyes-Coronado, D.; Rodríguez-Gattorno, G.; Espinosa-Pesqueira, M. E.; Cab, C.; de Coss, R.; Oskam, G. Phase-Pure TiO_2 Nanoparticles: Anatase, Brookite and Rutile. *Nanotechnology* **2008**, *19*, No. 145605.
(36) Staehelin, J.; Hoigné, J. Decomposition of Ozone in Water in the Presence of Organic Solutes Acting as Promoters and Inhibitors of Radical Chain Reactions. *Environ. Sci. Technol.* **1985**, *19*, 1206−1213.
(37) Nicolas, M.; Ndour, M.; Ka, O.; D'Anna, B.; George, C. Photochemistry of Atmospheric Dust: Ozone Decomposition on Illuminated Titanium Dioxide. *Environ. Sci. Technol.* **2009**, *43*, 7437−7442.
(38) Xu, Y.; Schoonen, M. A. A. The Absolute Energy Positions of Conduction and Valence Bands of Selected Semiconducting Minerals. *Am. Mineral.* **2000**, *85*, 543−556.
(39) Bulanin, K. M.; Lavalley, J. C.; Tsyganenko, A. A. IR Spectra of Adsorbed Ozone. *Colloids Surf., A* **1995**, *101*, 153−158.
(40) Li, W.; Gibbs, G. V.; Oyama, S. T. Mechanism of Ozone Decomposition on a Manganese Oxide Catalyst. 1. In Situ Raman Spectroscopy and Ab Initio Molecular Orbital Calculations. *J. Am. Chem. Soc.* **1998**, *120*, 9041−9046.
(41) Li, W.; Oyama, S. T. Mechanism of Ozone Decomposition on a Manganese Oxide Catalyst. 2. Steady-State and Transient Kinetic Studies. *J. Am. Chem. Soc.* **1998**, *120*, 9047−9052.
(42) Bulanin, K. M.; Lavalley, J. C.; Tsyganenko, A. A. Infrared Study of Ozone Adsorption on TiO_2 (Anatase). *J. Phys. Chem. A* **1995**, *99*, 10294−10298.
(43) Ostaszewski, C. J.; Stuart, N. M.; Lesko, D. M. B.; Kim, D.; Lueckheide, M. J.; Navea, J. G. Effects of Coadsorbed Water on the Heterogeneous Photochemistry of Nitrates Adsorbed on TiO_2. *J. Phys. Chem. A* **2018**, *122*, 6360−6371.
(44) George, S.; Pokhrel, S.; Ji, Z.; Henderson, B. L.; Xia, T.; Li, L.; Zink, J. I.; Nel, A. E.; Mädler, L. Role of Fe Doping in Tuning the Band Gap of TiO_2 for the Photo-Oxidation-Induced Cytotoxicity Paradigm. *J. Am. Chem. Soc.* **2011**, *133*, 11270−11278.
(45) Zhou, M.; Yu, J.; Cheng, B. Effects of Fe-Doping on the Photocatalytic Activity of Mesoporous TiO_2 Powders Prepared by an Ultrasonic Method. *J. Hazard. Mater.* **2006**, *137*, 1838−1847.
(46) Hurum, D. C.; Agrios, A. G.; Gray, K. A.; Rajh, T.; Thurnauer, M. C. Explaining the Enhanced Photocatalytic Activity of Degussa P25 Mixed-Phase TiO_2 Using EPR. *J. Phys. Chem. B* **2003**, *107*, 4545−4549.
(47) Zaki, M. I.; Fouad, N. E.; Mekhemer, G. A. H.; Jagadale, T. C.; Ogale, S. B. TiO_2 Nanoparticle Size Dependence of Porosity, Adsorption and Catalytic Activity. *Colloids Surf., A* **2011**, *385*, 195−200.
(48) Schneider, J.; Matsuoka, M.; Takeuchi, M.; Zhang, J.; Horiuchi, Y.; Anpo, M.; Bahnemann, D. W. Understanding TiO_2 Photocatalysis: Mechanisms and Materials. *Chem. Rev.* **2014**, *114*, 9919−9986.
(49) Pan, J.; Liu, G.; Lu, G. Q.; Cheng, H.-M. On the True Photoreactivity Order of {001}, {010}, and {101} Facets of Anatase TiO_2 Crystals. *Angew. Chem., Int. Ed.* **2011**, *50*, 2133−2137.
(50) Luttrell, T.; Halpegamage, S.; Tao, J.; Kramer, A.; Sutter, E.; Batzill, M. Why Is Anatase a Better Photocatalyst than Rutile? - Model Studies on Epitaxial TiO_2 Films. *Sci. Rep.* **2014**, *4*, No. 4043.

https://dx.doi.org/10.1021/acs.est.0c05861
Environ. Sci. Technol. 2020, 54, 13509−13516

(51) Gao, L.; Zhang, Q. Effects of Amorphous Contents and Particle Size on the Photocatalytic Properties of TiO_2 Nanoparticles. *Scr. Mater.* **2001**, *44*, 1195−1198.
(52) Miao, J.; Zhang, R.; Zhang, L. Photocatalytic Degradations of Three Dyes with Different Chemical Structures Using Ball-Milled TiO_2. *Mater. Res. Bull.* **2018**, *97*, 109−114.
(53) Ohtani, B.; Mahaney, O. O. P.; Amano, F.; Murakami, N.; Abe, R. What Are Titania Photocatalysts?—An Exploratory Correlation of Photocatalytic Activity with Structural and Physical Properties. *J. Adv. Oxid. Technol.* **2016**, *13*, 247−261.
(54) Ndour, M.; D'Anna, B.; George, C.; Ka, O.; Balkanski, Y.; Kleffmann, J.; Stemmler, K.; Ammann, M. Photoenhanced Uptake of NO_2 on Mineral Dust: Laboratory Experiments and Model Simulations. *Geophys. Res. Lett.* **2008**, *35*, No. L05812.
(55) Hanisch, F.; Crowley, J. N. Ozone Decomposition on Saharan Dust: An Experimental Investigation. *Atmos. Chem. Phys.* **2003**, *3*, 119−130.
(56) Ji, Z.; Wang, G.; Yu, M.; Pal, J. S. Potential Climate Effect of Mineral Aerosols over West Africa: Part II—Contribution of Dust and Land Cover to Future Climate Change. *Clim. Dyn.* **2018**, *50*, 2335−2353.
(57) Journet, E.; Desboeufs, K. V.; Caquineau, S.; Colin, J.-L. Mineralogy as a Critical Factor of Dust Iron Solubility. *Geophys. Res. Lett.* **2008**, *35*, No. L07805.
(58) Caquineau, S.; Gaudichet, A.; Gomes, L.; Magonthier, M.-C.; Chatenet, B. Saharan Dust: Clay Ratio as a Relevant Tracer to Assess the Origin of Soil-Derived Aerosols. *Geophys. Res. Lett.* **1998**, *25*, 983−986.
(59) Atkinson, J. D.; Murray, B. J.; Woodhouse, M. T.; Whale, T. F.; Baustian, K. J.; Carslaw, K. S.; Dobbie, S.; O'Sullivan, D.; Malkin, T. L. The Importance of Feldspar for Ice Nucleation by Mineral Dust in Mixed-Phase Clouds. *Nature* **2013**, *498*, 355−358.
(60) Kebede, M. A.; Bish, D. L.; Losovyj, Y.; Engelhard, M. H.; Raff, J. D. The Role of Iron-Bearing Minerals in NO_2 to HONO Conversion on Soil Surfaces. *Environ. Sci. Technol.* **2016**, *50*, 8649−8660.
(61) Engelbrecht, J. P.; Moosmüller, H.; Pincock, S.; Jayanty, R. K. M.; Lersch, T.; Casuccio, G. Technical Note: Mineralogical, Chemical, Morphological, and Optical Interrelationships of Mineral Dust Re-Suspensions. *Atmos. Chem. Phys.* **2016**, *16*, 10809−10830.
(62) Mishra, M.; Chun, D.-M. α-Fe_2O_3 as a Photocatalytic Material: A Review. *Appl. Catal., A Gen.* **2015**, *498*, 126−141.
(63) Chen, H.; Navea, J. G.; Young, M. A.; Grassian, V. H. Heterogeneous Photochemistry of Trace Atmospheric Gases with Components of Mineral Dust Aerosol. *J. Phys. Chem. A* **2011**, *115*, 490−499.

https://dx.doi.org/10.1021/acs.est.0c05861
Environ. Sci. Technol. 2020, 54, 13509−13516